UC Irvine
UC Irvine Previously Published Works

Title

Field-induced spin reorientation in Eu2CuO4:Gd studied by magnetic resonance

Permalink

https://escholarship.org/uc/item/9j02063b

Journal

Physical Review B, 48(22)

ISSN

2469-9950

Authors

Fainstein, A
Butera, A
Zysler, RD
et al.

Publication Date

1993-12-01

DOI

10.1103/physrevb.48.16775

Copyright Information

Peer reviewed

Field-induced spin reorientation in Eu_2CuO_4:Gd studied by magnetic resonance

A. Fainstein,* A. Butera, R. D. Zysler,† and M. Tovar
Centro Atómico Bariloche and Instituto Balseiro,‡ Comisión Nacional de Energía Atómica,
8400 San Carlos de Bariloche, Río Negro, Argentina

C. Rettori, D. Rao, and S. B. Oseroff
San Diego State University, San Diego, California 92182

Z. Fisk
Los Alamos National Laboratory, Los Alamos, New Mexico 87545

S-W. Cheong
AT&T Bell Laboratories, Murray Hill, New Jersey 07974

D. C. Vier and S. Schultz
University of California San Diego, San Diego, California 92037
(Received 20 July 1993)

We report a magnetic-resonance study of Gd-doped Eu_2CuO_4 single crystals. Cooling the samples in a magnetic field H_{FC}, induces weak ferromagnetism (WF), with a strong out-of-plane anisotropy determined by the Dzyaloshinsky-Moriya (DM) interaction. In addition, there is in-plane anisotropy with an easy-axis parallel to the [110] crystal axis closest to H_{FC}. An intense resonance mode is observed at the X band (9.5 GHz) when H_{FC} is applied parallel to one of the $\langle 110 \rangle$ axes and the measuring field is rotated by 90° in the CuO_2 plane. At the Q band (35 GHz), the in-plane resonance modes strongly depend on angle and temperature. We analyze the experimental results in terms of a phenomenological model for the magnetic free energy, which predicts a reorientation transition of the WF component of the magnetization m_{WF} induced by the external field. Associated with this transition, a softening of the WF magnetic resonance mode occurs when the external field is applied perpendicular to the easy magnetization axis. The resulting angular variation of the resonance modes depends on whether the energy gap for the magnetic excitations is larger or smaller than the microwave energy. From the resonance data we have determined both the out-of-plane and in-plane anisotropy fields, $H_{DM}(T)$ and $H_{ax}(T)$, respectively. The extrapolated values for $T=0$ are $H_{DM}(0)=3.5(5)\times10^5$ G and $H_{ax}(0)=12(2)$ G. Both anisotropy fields decrease with increasing T, vanishing around $T_N \cong 243$ K. The temperature dependence of the peak-to-peak linewidths, ΔH_{pp}, measured at the X and Q bands is explained in terms of a temperature-independent frequency linewidth, $\Delta\omega_{1/2}/\gamma=1.6(2)$ kG. Nonresonant absorption losses around the maxima and minima of the ω/γ vs H curves are also described in terms of this finite width for the resonance modes.

I. INTRODUCTION

Antiferromagnetic (AF) order of the copper moments is present in the rare-earth cuprates R_2CuO_4, below $T_N \cong 240-280$ K.[1] In addition, weak ferromagnetism (WF) associated with a canting of the Cu moments away from perfect AF alignment has been reported for the rare earths with smaller ionic radii.[2] A composition boundary for WF in the cuprates has been established[2] near Eu_2CuO_4. In solid solutions, including two different rare-earth ions, WF appears for compounds with lattice parameters similar to those of Eu_2CuO_4, such as[3] $SmGdCuO_4$ and[4] $(Nd_{0.375}Gd_{0.625})_2CuO_4$.

The R_2CuO_4 cuprates form in the tetragonal,[5] Nd_2CuO_4-type crystal structure (T' phase). For the WF compounds, the existence of lattice distortions has been proposed in order to explain the x-ray and Mössbauer data[4] for $(Nd_{1-x}Gd_x)_2CuO_4$, the splitting of the electron paramagnetic resonance[6] (EPR) of Gd^{3+} ions diluted in Eu_2CuO_4, the anomalously large thermal parameters in the x-ray-diffraction spectrum[7,8] for Gd_2CuO_4 and Tm_2CuO_4, and the differences between the Raman scattering of Gd_2CuO_4 and the lighter rare-earth cuprates.[9] These distortions have been proposed as displacements of the oxygen ions in the CuO_2 planes away from the highly symmetric positions O(1) in the T' structure. The estimated average values are 0.18 Å for Gd_2CuO_4 (Ref. 7) and 0.36 Å for Tm_2CuO_4 (Ref. 8). These displacements lower the symmetry of the Cu-O(1)-Cu bonds and the existence of a nonvanishing antisymmetric exchange interaction between Cu moments is then allowed.[10,11] These distortions seem to be disordered in the case of compounds near the WF boundary. In contrast, superstructure reflections suggesting an

ordered displacement of the oxygen ions have been observed in electron-diffraction experiments on the heavier rare-earth cuprates.[8]

For the compounds near the boundary, a strong dependence on the magnetothermal history of the samples has also been reported. The splitting of the EPR lines of diluted Gd^{3+} ions in Eu_2CuO_4, observed below the ordering temperature of the copper moments, was shown[6] to be dependent on the intensity and orientation of the magnetic field H_{FC}, applied while cooling the samples through the Néel temperature T_N.

A microwave absorption signal (MAS) has been reported in Ref. 12 for Eu_2CuO_4 single crystals. This signal, as measured at 9.2 GHz, presents a strong out-of-plane anisotropy, similar to that found in Gd_2CuO_4 crystals.[2] Besides, it exhibits an unusual in-plane anisotropy. For field-cooled (FC) samples, with H_{FC} oriented along one of the $\langle 110 \rangle$ directions in the CuO_2 planes, the signal was only observed for the dc-measuring magnetic field applied perpendicular to H_{FC}. Recent measurements of the dc magnetization in slightly doped Eu_2CuO_4 crystals[13] have shown that a WF component develops for FC samples below $T_N \cong 243$ K, with a uniaxial anisotropy axis oriented along the $\langle 110 \rangle$ direction closest to H_{FC}.

In this work we present detailed measurements of the microwave spectra at two different frequencies, which show that the MAS in Eu_2CuO_4 may be described in terms of magnetic resonances associated with the ordered Cu lattice. In Sec. II we describe the experimental setup. In Sec. III we present a phenomenological model for the free energy of the magnetic system which explains the experimental results presented and discussed in Sec. IV, as well as the preliminary results reported in Ref. 12. The conclusions are given in Sec. V.

II. EXPERIMENTAL DETAILS

Eu_2CuO_4 single crystals were grown following standard flux techniques, either in Pt or Al_2O_3 crucibles.[14] Samples slightly doped with Gd ions (less than 1 at. %) were also grown using the same techniques. In all cases the crystals grew in the shape of small platelets with the c axis oriented perpendicular to the platelets.

Measurements at the X band (9.4 GHz) were made in a Bruker ESP-300 EPR spectrometer and at the Q band (35.0 GHz) in a modified V-4500 Varian EPR spectrometer. The measurements were made between 10 and 300 K for the X band and between 55 and 300 K for the Q band. The X-band spectrometer was operated either in the absorption or the dispersion mode. The Q-band spectrometer was operated only in the absorption mode. A rectangular TE_{102} cavity was used for the X-band measurements and the Q-band experiments were carried on in a cylindrical TE_{011} cavity. Since a component of the microwave field parallel to the CuO_2 planes is needed for the excitation of the low-field absorptions,[12] we have located the sample along the cavity axis but away from its center. The modulation coils are fixed to the microwave cavity in both cases. In the X-band experiments, the angular variations were measured by rotating the sample. Since in the Q band this method results in large varia-

tions of the cavity coupling, the external field was rotated instead. Because the modulation coils are fixed to the cavity, the angle between the external and the modulation fields varies and the signals are then subjected to angular modulation besides the normal amplitude modulation of the external field.[15] The effects of angular modulation on highly anisotropic signals are large and need to be taken into account.

As reported in Ref. 12, the MAS for Eu_2CuO_4 is sample dependent. We have found no MAS signal (or WF component of the dc magnetization) for undoped crystals grown in Al_2O_3 crucibles. On the other hand, we have observed MAS for undoped samples grown in Pt crucibles and for samples slightly doped with Gd, grown either in Al_2O_3 or Pt crucibles. Since Eu_2CuO_4 lies on the boundary for WF in the R_2CuO_4 series[2,3] we interpret this observation as due to the need of a small shift of the system toward smaller lattice parameters in order to observe WF. For example, $Eu_{1.8}Gd_{0.2}CuO_4$ presents fully developed WF as reported in Ref. 2. Where MAS was seen, a similar behavior was observed for all the systems studied. The measurements presented here correspond to a sample containing 1 at. % Gd, for which the MAS had a good signal-to-noise ratio.[16]

III. THEORETICAL FRAMEWORK

A. Magnetic model

The appearance of an intense resonant absorption at the X band,[12] at a field close to the anisotropy critical field, $H_c \cong 340$ G for $T = 135$ K, deduced from the dc-magnetization data in Ref. 13, resembles the softening of modes observed by Hagedorn *et al.*[17] in the spin reorientation transition for the canted antiferromagnet $TmFeO_3$. In that case, a resonant absorption was observed only when the magnetic field was applied perpendicular to the anisotropy easy axis, at the critical field needed to rotate the WF component from the easy axis to a direction perpendicular to it.

A two-sublattice model can be used[13,17–21] to calculate the equilibrium position of the magnetization vectors and the resonance frequencies for WF systems. A phenomenological free energy, including second-order anisotropy terms, may be written as[18]

$$2\mathcal{F} = \lambda \mathbf{M}_1 \times \mathbf{M}_2 + K_{az}\mathbf{M}_{1z}^2 + K_{az}\mathbf{M}_{2z}^2 + K_{ax}\mathbf{M}_{1x}^2$$
$$+ K_{ax}\mathbf{M}_{2x}^2 + \mathbf{D} \cdot (\mathbf{M}_1 \times \mathbf{M}_2) - (\mathbf{M}_1 + \mathbf{M}_2) \cdot \mathbf{H} , \quad (1)$$

where $\mathcal{F}$ is the free energy per mole, $\lambda > 0$ describes the AF coupling between the two Cu magnetic lattices $\mathbf{M}_1$ and $\mathbf{M}_2$, $K_{az} > 0$ indicates an out-of-plane magnetic anisotropy energy favoring the orientation of the Cu moments within the ab plane (Ref. 22), $K_{ax} < 0$ corresponds to the in-plane anisotropy, where $\hat{x}$ is parallel to one of the $\langle 110 \rangle$ directions,[13] and $\mathbf{D} \cdot (\mathbf{M}_1 \times \mathbf{M}_2)$ is the Dzyaloshinsky-Moriya (DM) antisymmetric interaction[10] which gives rise to a WF component, with $\mathbf{D} = D\hat{z}$ as discussed previously.[11] The last term corresponds to the Zeeman energy.

The static equilibrium conditions in the AF phase, with the constraint $|\mathbf{M}_1|=|\mathbf{M}_2|=M_0=$const, are set by $\partial\mathcal{F}/\partial\mathbf{M}_\nu\times\mathbf{M}_\nu=0$, with $\nu=1,2$. The anisotropy energy (with $K_{az}>0$) favors an easy plane for $\mathbf{M}_1$ and $\mathbf{M}_2$, which are almost in opposite directions due to their strong AF interaction, with a small canting of the Cu moments induced by the DM interaction. For H applied in the ab plane, the staggered magnetization, $l=(\mathbf{M}_1-\mathbf{M}_2)/2$, and the uniform magnetization, $\mathbf{m}=(\mathbf{M}_1+\mathbf{M}_2)/2$, remain in this plane. Their magnitudes and orientation within the plane are given by

$$l\equiv|l|\simeq M_0 \ ,\tag{2a}$$

$$m\equiv|\mathbf{m}|\simeq m_{WF}=(H_{DM}/2H_E)M_0 \ ,\tag{2b}$$

$$(H_{DM}/2H_E)H\sin(\varphi-\alpha)=(H_{ax}/2)\sin(2\alpha) \ ,\tag{2c}$$

when $H_E\gg H_{DM}\gg(H,H_{ax})$, where $H_E=\lambda M_0$ is the exchange field, $H_{DM}=DM_0$, and $H_{ax}=2K_{ax}M_0$. The angles φ and α are defined in Fig. 1.

In this case l reaches almost its maximum value, $l=M_0$. The small canting of the AF sublattices gives rise to a WF component m_{WF} whose magnitude is almost independent of the applied field H and given by Eq. (2b). The orientation of m_{WF} is determined by Eq. (2c) when an external field is applied. At zero field, m_{WF} is parallel to $\hat{y}$ and when H is applied parallel to $\hat{x}$, m_{WF} starts to rotate and aligns with H at a critical field, $H_C=(2H_E/H_{DM})H_{ax}$.

The Cu sublattice magnetization has been determined for the isostructural compounds Pr_2CuO_4 and Nd_2CuO_4, from neutron-scattering measurements.[23] The extrapolated value for $T=0$ is $M_0(0)=0.4(1)\ \mu_B$/Cu atom. The AF superexchange interaction for Eu_2CuO_4, $J_{NN}\cong115$ meV, has been estimated from the two-magnon Raman scattering.[24] This value may be related to the macroscopic exchange field H_E through the relation $g\mu_B H_E=zJ_{NN}S$, where $z=4$, $g=2.2$, and S is reduced from $\frac{1}{2}$ by a factor 0.63 due to quantum renormalization.[22] This gives for $T=0$, $H_E(0)=1.14\times10^7$ G.
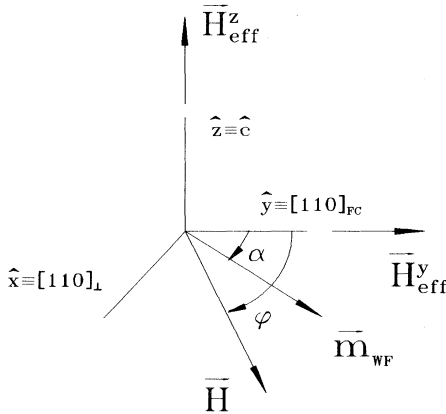

FIG. 1. Relative orientation of the WF component m_{WF}, the anisotropy fields H^y_{eff} and H^z_{eff}, and the external field H, with respect to the crystallographic axes. Here, $[110]_{FC}$ indicates the $\langle110\rangle$ direction closest to the field for cooling H_{FC}.

From neutron-scattering experiments, an out-of-plane anisotropy field, $H_{az}=2K_{az}M_0\cong1$ kG, has been estimated[22] for La_2CuO_4. We may expect the same order of magnitude for H_{az} in our case. The in-plane anisotropy field H_{ax} may be derived using the anisotropy constants determined from dc-magnetization measurements.[13] For $T=135$ K we obtain $H_{ax}\cong4(1)$ G.

H_{DM} may be estimated from the WF component measured in Ref. 13, using Eq. (2b). From the extrapolated value[13] for $T=0$, $m_{WF}(0)=5.0(5)\times10^{-3}\mu_B$/Cu atom, and neglecting contributions from the Van Vleck paramagnetism of the Eu^{3+} lattice, we obtain $H_{DM}(0)\cong3(1)\times10^5$ G. The order of magnitude of these results confirms the approximations made when deriving Eqs. (2). The applied field at resonance was always less than 1 kG in our experiments.

B. Magnetic-resonance modes

The resonance frequencies of the system are obtained after linearizing the equations of motion $\partial\mathbf{M}_\nu/\partial t=\gamma(\partial\mathcal{F}/\partial\mathbf{M}_\nu)\times\mathbf{M}_\nu$, where $\nu=1,2$ and γ is the gyromagnetic factor for the Cu moments. Two resonance modes are obtained:[18] a high-frequency AF mode and a low-frequency WF mode. Their frequencies at $H=0$ are given by $(\omega/\gamma)^2\cong H^2_{DM}+2H_E H_{az}$ and $(\omega/\gamma)^2\cong2H_E H_{ax}$, respectively. For the values of the effective fields previously derived, the AF mode is expected to occur at ≈30 cm^{-1} for $T=0$ and the WF mode in the microwave region (≈1 cm^{-1}). For the microwave energies used in this work, small compared with that of the AF mode, the two magnetic lattices move almost rigidly. Then, an effective free energy may be written for the uniform magnetization $\mathbf{m}$ as

$$\mathcal{F}_{eff}=K^y_{eff}m^2_y+K^z_{eff}m^2_z-\mathbf{m}\cdot\mathbf{H} \ .\tag{3}$$

$\mathcal{F}_{eff}$ is equivalent to $\mathcal{F}$ for describing the equilibrium and the low-energy excitations of the system,[21] having the following relations between their parameters:

$$H^y_{eff}=2K^y_{eff}m_{WF}=(2H_E/H_{DM})H_{ax} \ ,$$
$$H^z_{eff}=2K^z_{eff}m_{WF}=H_{DM}+(H_{DM}/2H_E)H_{az} \ .\tag{4}$$

Notice that the high-energy AF mode is lost on reducing $\mathcal{F}$ to $\mathcal{F}_{eff}$. However, $\mathcal{F}_{eff}$ is simpler and requires only two parameters, H^y_{eff} and H^z_{eff}, in order to describe the static and dynamic properties of the WF component. Equation (4) shows that the antisymmetric exchange field H_{DM} acts as an additional source for the strong easy-plane magnetic anisotropy. In terms of these effective magnetic fields, the critical field for spin reorientation is given by $H_C=H^y_{eff}$.

From Eq. (3) the frequency of the WF mode is derived as follows:

$$(\omega/\gamma)^2=H^2+H[(2H^y_{eff}+H^z_{eff})\cos\alpha_0\cos\varphi$$
$$+(H^z_{eff}-H^y_{eff})\sin\alpha_0\sin\varphi]$$
$$+H^y_{eff}(H^y_{eff}+H^z_{eff})\cos^2\alpha_0-H^y_{eff}H^z_{eff}\sin^2\alpha_0\tag{5}$$

where α_0 is the equilibrium value determined by Eq. (2c).

Simple analytical expressions exist for the limiting cases $\varphi=0°$ and $\varphi=90°$. For $\varphi=0°$, Eqs. (2) and (5) give

$$(\omega_\parallel/\gamma)^2=H^2+H(2H_{\text{eff}}^y+H_{\text{eff}}^z)+H_{\text{eff}}^y(H_{\text{eff}}^y+H_{\text{eff}}^z), \quad (6)$$

while for $\varphi=90°$ the resonance frequency is given by

$$(\omega_\perp/\gamma)^2=H_{\text{eff}}^y(H_{\text{eff}}^y+H_{\text{eff}}^z)-H^2(1+H_{\text{eff}}^z/H_{\text{eff}}^y),$$

$$\text{if } H<H_C=H_{\text{eff}}^y,$$

$$(7)$$

$$(\omega_\perp/\gamma)^2=H^2+H(H_{\text{eff}}^z-H_{\text{eff}}^y)-H_{\text{eff}}^yH_{\text{eff}}^z,$$

$$\text{if } H\geq H_C=H_{\text{eff}}^y.$$

IV. RESULTS AND DISCUSSION

A. *X*-band measurements

We have confirmed for the chosen Eu_2CuO_4:Gd sample, all the properties reported in Ref. 12 for the *X*-band spectrum of undoped Eu_2CuO_4 and in Ref. 13 for the dc magnetization, namely: (i) Cooling in a field H_{FC} determines the appearance of a WF component of the magnetization, m_{WF}, below T_N. This component lies in the *ab* plane and its magnitude increases with decreasing temperature, with an extrapolated value for $T=0$, $m_{WF}(0)\approx5\times10^{-3}\mu_B$/Cu atom. In-plane anisotropy is present, with a preferred axis along the $\langle110\rangle$ direction closest to H_{FC}, which we identify here as $[110]_{FC}$. (ii) A MAS signal is observed in FC samples with strong out-of-plane anisotropy; the field position and width of the line follow a $1/\sin\theta$ dependence, with θ being the angle between the applied field **H** and the *c* axis. (iii) No signal is detected in zero-field-cooled (ZFC) samples. In FC samples the amplitude of the MAS, measured at the same temperature, increases with H_{FC} and saturates for $H_{FC}\geq15$ kG. The results presented in this work correspond to $H_{FC}=15$ kG. (iv) The signal can be seen only when the microwave magnetic field $\mathbf{h}_{rf}$ is oriented both perpendicular to the external dc field and parallel to the CuO_2 planes. (v) Within the *ab* plane, the MAS is very intense only for $\mathbf{H}\perp[110]_{FC}$. We call this orientation $\mathbf{H}\parallel[110]_\perp$. The amplitude of this absorption decreases rapidly when **H** is rotated away from $[110]_\perp$. We have also found that heating the sample up to a temperature T_h and cooling it back in zero field to the original temperature does not change the MAS if $T_h\leq220$ K. For $T_h\geq220$ K, the intensity of the signal measured at low temperatures decreases (as compared to the FC sample) with increasing T_h and vanishes when $T_h\geq250$ K.

We have analyzed the resonant nature of the MAS by measuring, under the same conditions, the real (dispersive) part, $\chi'(H)$, and the imaginary (absorption) part, $\chi''(H)$, of the dynamic susceptibility. We have found that $\chi''(H)$, as determined by integration of the measured signal in the absorption mode, presents a single maximum at a field H_r. For $\mathbf{H}\parallel[110]_\perp$ and $T\cong77$ K, we measured $H_r\approx470(10)$ G, a value somewhat smaller than that reported[12] for undoped Eu_2CuO_4. As in that case, $H_r(T)$ varies slowly with temperature for $T\leq200$ K, with a minimum value for $T\cong130$ K. H_r increases rapidly both
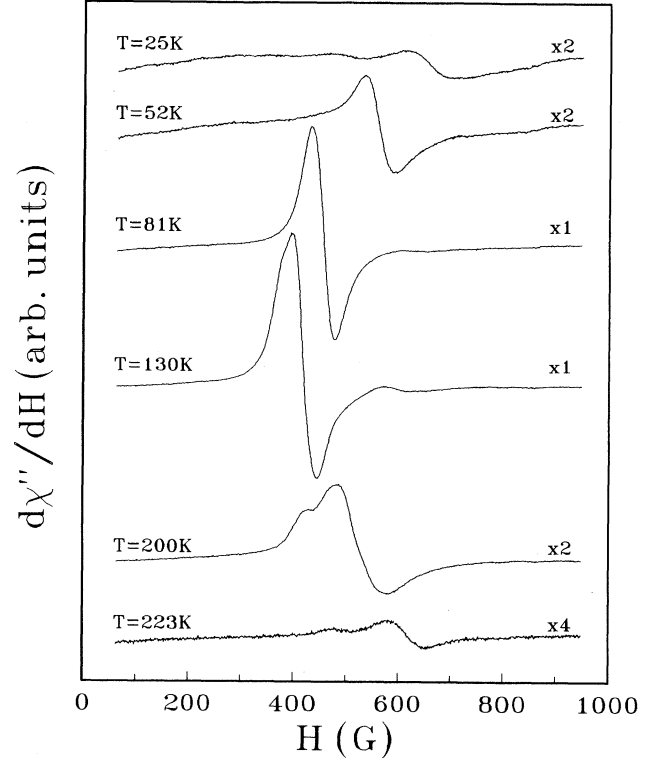

FIG. 2. *X*-band MAS measured at different temperatures for $\mathbf{H}\parallel[110]_\perp$.

above ≈200 K and below 50 K, as shown in Fig. 2. The MAS presents also a minimum linewidth, $\Delta H_{pp}\approx50$ G, at $T\approx130$ K, showing some unresolved structure. Above 200 K, the linewidth increases rapidly, reaching $\Delta H_{pp}\approx200$ G at 230 K. At low T the linewidth also increases, up to $\Delta H_{pp}\approx100$ G for $T\cong15$ K. The signal shows maximum amplitude at ≈130 K and then decreases with increasing T, vanishing at about 235 K. For $T<130$ K, the intensity decreases with decreasing T and the signal was not detected below $T\approx13$ K.

After integration, the signal measured in the dispersion mode is proportional to $\chi'(H)$ and presents a single maximum for **H** away from $[110]_\perp$, as shown in Fig. 3 for

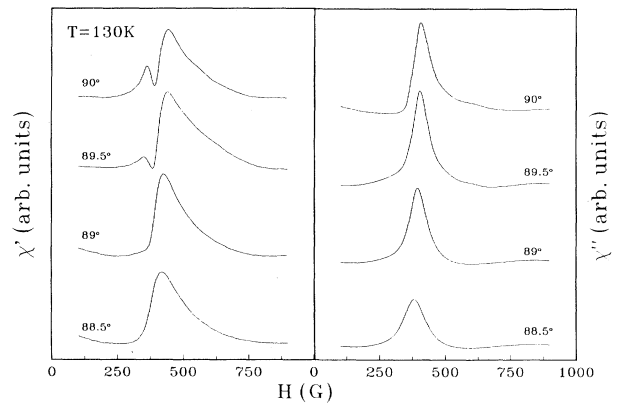FIG. 3. Integrated signals for the *X* band in the dispersion (χ') and absorption (χ'') modes of the spectrometer.

$T = 130$ K. This is at variance with the usual appearance of zeros for $\chi'(H)$ in correspondence with the maxima of $\chi''(H)$. This observation suggests that the magnetic system does not reach the exact resonance conditions, and microwave losses (nonresonant in character) are present only because of the finite width of the resonance modes, as discussed in Ref. 17 for the case of TmFeO$_3$. For **H** very near $[110]_\perp$ instead, although $\chi'(H)$ does not reach zero, a dip is observed for $H \cong H_r$ (see Fig. 3), indicating the possibility of resonant behavior for this particular orientation of **H**. This will be discussed in Sec. IV C.

B. Q-band measurements

For data taken at the Q band, the MAS presence or absence also depends on the cooling conditions. The $\mathbf{H}\|[110]_{\mathrm{FC}}$ continues to be a preferred orientation in FC samples, although intense signals have been observed for **H** within the ab plane in a much wider angular range than for the X band. Another important difference found in the Q band is that two lines instead of one are measured at the lowest temperatures. These lines were observed at about 135 and 850 G, for $\mathbf{H}\|[110]_\perp$ and $T = 80$ K. In Fig. 4 we present data taken for **H** oriented 12° away from $[110]_\perp$ at different temperatures. The behavior observed for this orientation is qualitatively similar to that for $\mathbf{H}\|[110]_\perp$, but we have chosen this direction because the signals are more intense and the
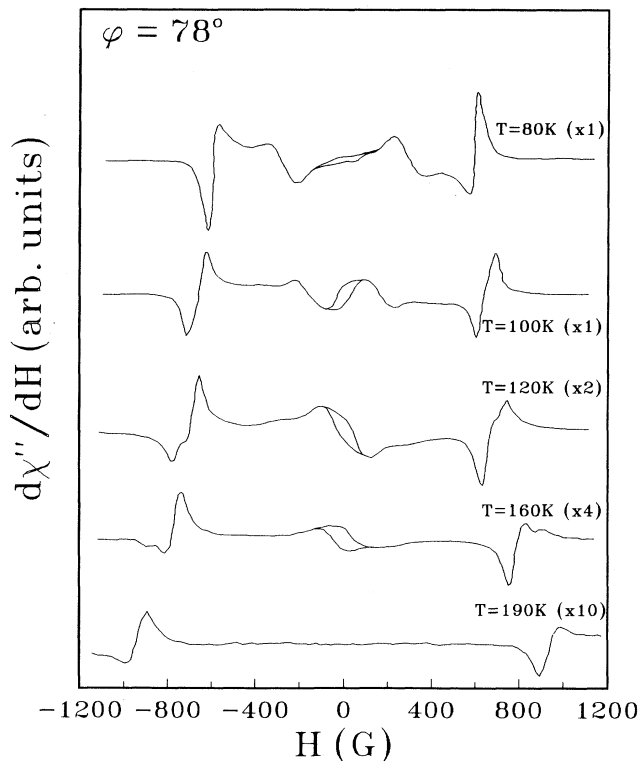
FIG. 5. H_r vs T, as measured at the Q band for different values of φ. $T_{\mathrm{GQ}} \cong 107(5)$ K indicates the temperature where the anisotropy gap ω_G equals the microwave energy ω_Q.

spectra show more clearly the characteristics we want to stress. The spectra are symmetric with respect to $\mathbf{H} = 0$, although showing some hysteresis in magnetic-field loops. As T increases, the signal at the lower field shifts toward $H = 0$ and finally merges with the symmetric line from negative fields at a characteristic temperature, $T_{\mathrm{GQ}} \cong 107(5)$ K. As the temperature continues to increase, the signal at zero field decreases and disappears at ≈ 170

FIG. 4. Q-band signals at different temperatures for $\varphi = 78°$, i.e., **H** oriented 12° away from $[110]_\perp$. For this orientation the spectra are very similar to those for $\mathbf{H}\|[110]_\perp$, but angular modulation provides better signal to noise ratios.
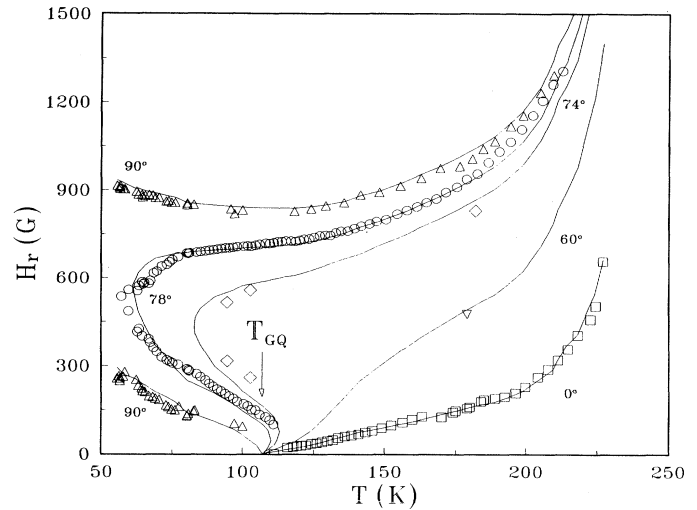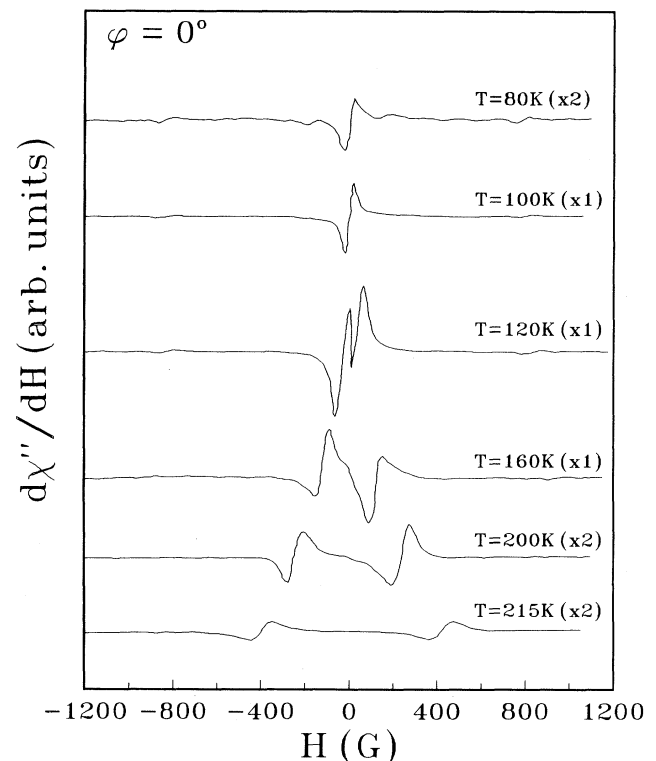
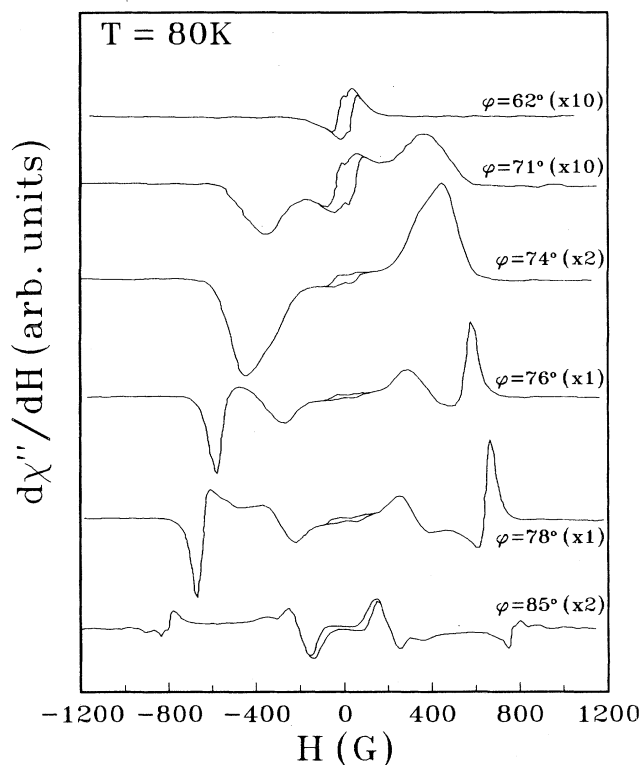FIG. 6. Q-band signals at different temperatures for $\varphi = 0°$, i.e., $\mathbf{H}\|[110]_{\mathrm{FC}}$.

FIG. 7. Angular dependence of the Q-band signals for $T=80$ K. Notice the particular shape of the signal in the φ interval $(67°, 74°)$ and the opposite phase of the signals for $\varphi > 74°$, due to angular modulation of the external field.

K. The line at 850 G slowly moves to higher fields and its linewidth increases with increasing T. Simultaneously, its intensity is reduced and the signal disappears at $T \approx 210$ K. The temperature dependence of the center fields of these lines[25] is shown in Fig. 5.

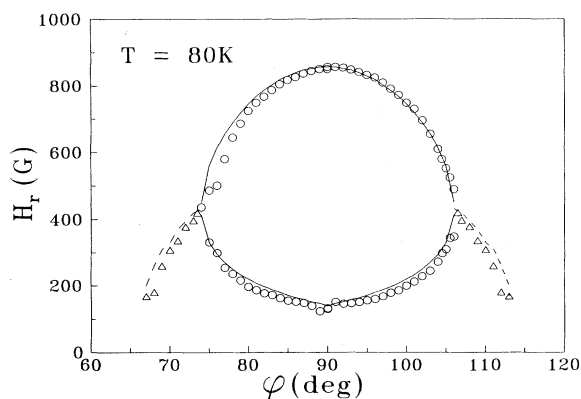Below T_{GQ} and for $\mathbf{H} \| [110]_{FC}$, a single line at $H \cong 0$ is

FIG. 8. $H_r(\varphi)$ vs φ, as measured at the Q band for $T=80$ K (circles). The continuous line corresponds to a fit to Eq. (5). The triangles represent the fields for maximum amplitude of the nonresonant signal in the range from $67° \le \varphi \le 74°$. The dashed lines correspond to the calculated values of H_{min}, the field where the ω/γ vs H curves present a minimum.
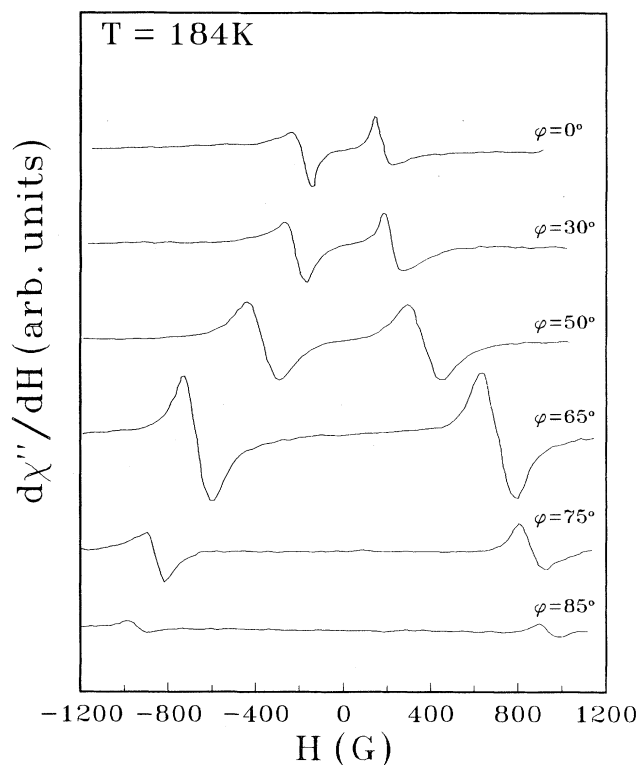
FIG. 9. Angular dependence of the Q-band signals for $T=184$ K.

observed. Its intensity increases with T and at T_{GQ} it starts to split into two lines, symmetric with respect to $H=0$, as seen in Fig. 6. As T continues to increase, each line slowly shifts to higher values of $|H|$, as seen in Fig. 5. Above $T \cong 200$ K the intensity of the spectrum decreases again, disappearing at $T \approx 230$ K.

In Fig. 7 we present the spectra taken at 80 K for different orientations of $\mathbf{H}$ in the ab plane. As already mentioned, only a very small feature is detected around zero field when $\varphi=0°$, with φ being the angle between $\mathbf{H}$ and $[110]_{FC}$ (see Fig. 1). When φ increases, this signal
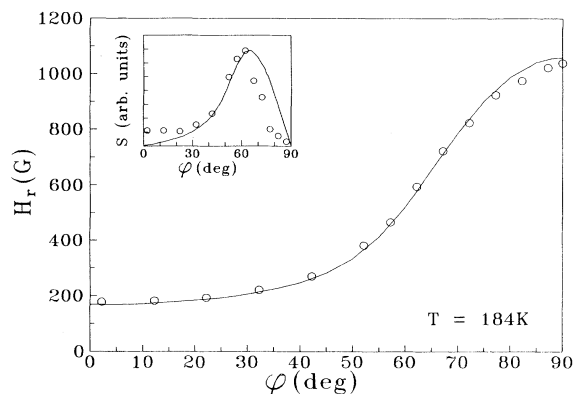

FIG. 10. $H_r(\varphi)$ vs φ, as measured in the Q band for $T=184$ K. The continuous line corresponds to a fit to Eq. (5). The inset shows the relative amplitude S of the detected signal. The continuous line in the inset corresponds to the normalized derivative $\partial H_r(\varphi)/\partial \varphi$.

remains almost unchanged up to $\varphi \cong 67°$. At this angle a broad line develops at $H \cong 160$ G, which shifts to higher fields, increasing its amplitude as φ increases. Notice that this line does not cross the base line, i.e., does not reach zero. In Fig. 8 we represent with triangles the fields where this signal has its maximum amplitude. For $\varphi > 74°$ it splits into two lines with opposite phase. One of them moves to higher and the other to lower fields. The maximum splitting is reached for $\varphi = 90°$, i.e., when $\mathbf{H} \| [110]_\perp$. For $\varphi > 90°$, a specular behavior is observed. The fields where these two lines cross zero[25] are given in Fig. 8. In Fig. 9 we present the spectra taken at $T = 184$ K, a temperature higher than T_{GQ}. In this case, a single resonance line is observed for all values of φ in the ab plane. The fields for zero crossing are given in Fig. 10.

C. Analysis of the data

The Q-band experimental data taken at $T = 80$ K for $\varphi = 90°$ were fitted to Eq. (7), obtaining $H^y_{eff} = 4.5(4) \times 10^2$ G and $H^z_{eff} = 3.2(3) \times 10^5$ G. With these fitted parameters we have calculated the ω/γ vs H curves given in Fig. 11 for different values of φ.

According to Eq. (5), there is an excitation gap for the ferromagnetic mode at $H = 0$ given by $(\omega_G/\gamma) = \sqrt{H^y_{eff}(H^y_{eff} + H^z_{eff})}$, where the leading contribution[17] is $\sqrt{H^y_{eff} H_{DM}}$. At this temperature the calculated value of ω_G is larger than the microwave frequency at both the X band $(\omega_X/2\pi = 9.44$ GHz) and Q band $(\omega_Q/2\pi = 35.04$ GHz). Due to this fact a resonant absorption is not expected for $\varphi = 0°$ at any field since ω/γ increases monotonically with $|H|$ for this angle. However, because of the finite linewidth of the resonance modes, nonresonant microwave losses may be expected.[17] These losses should show a maximum near $H = 0$, where the ω/γ vs H curves present a minimum, i.e., the curves are closer to the microwave frequency. A similar behavior is predicted for all values of φ. However, $\partial(\omega/\gamma)/\partial H|_{H\to 0}$ decreases with increasing φ, going to zero for $\varphi = 90°$, where the minimum disappears. The line at $H = 0$ shown in Fig.
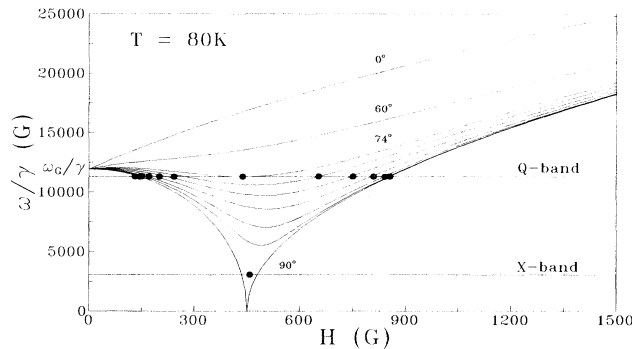

FIG. 11. ω/γ vs H curves for the WF resonant mode, calculated for different values of φ using Eq. (5). Intermediate curves between 74° and 90° correspond to 77°, 80°, 83°, 86°, and 88°. Horizontal lines indicate the microwave frequencies ω_x/γ and ω_Q/γ and the cirlces are the experimental data at both frequencies measured for $T = 80$ K.

6 for $\varphi = 0°$, can be observed up to $\varphi \approx 75°$ (see Fig. 7) and may be associated with this nonresonant absorption.

For $\varphi \cong 67°$, the WF mode starts to soften at a finite field as shown in Fig. 11, reaching a minimum energy at a field H_{min}. The frequency at this minimum ω_{min} decreases with increasing φ, while H_{min} increases. This minimum in the ω/γ vs H curves is expected to give rise to a second nonresonant absorption line around H_{min} while $\omega_{min} > \omega_Q$. The measured spectra at the Q band show, indeed, the appearance of a line at $H \cong 160$ G for $\varphi = 67°$. As predicted, this line shifts to higher fields as φ increases and it is observed as a single line up to $\varphi \cong 74°$. For reasons that will be discussed in Sec. IV D, we have taken H_{min} as the field for the maximum amplitude. Experimental and calculated values for H_{min} are compared in Fig. 8.

For $\varphi \cong 74°$, $\omega_{min} = \omega_Q$ at $H_{min} \cong 430$ G. Then, for $\varphi > 74°$, two separate absorption lines are expected at the Q band, one moving to higher and the other to lower fields. Again, the agreement between the predictions of the model and the experimental data is excellent, as seen in Fig. 8 where the continuous lines have been calculated using Eq. (5).

Figure 11 shows that ω_{min} continues to decrease with increasing φ and reaches zero for $\varphi = 90°$, at $H_{min} = H^y_{eff}$. This is the critical field H_C for the reorientation of $\mathbf{m}_{WF}$ in the ab plane. Under these conditions a strong signal is observed[12] at the X band. The resonance frequency changes rapidly with angle around $\varphi = 90°$, as seen in Fig. 11. By rotating the applied field by 2°, ω_{min} is already larger than ω_X and for this reason, a resonant absorption at the X band is only observed in a narrow region around $\varphi = 90°$. Nonresonant microwave losses may be observed in a larger angular interval, due to the finite linewidth of the resonance modes. The passage from nonresonant to resonant behavior in the microwave spectra as a function of the field orientation has been extensively described by Hagedorn et al.[17,21] for TmFeO$_3$. In that case, a resonance line was observed essentially at the same field from 5 to 54 000 MHz, due to a large anisotropy gap. In the case of Eu$_2$CuO$_4$, although conceptually similar, a richer behavior is present due to a much smaller in-plane anisotropy that reduces the magnitude of the energy gap. Although two resonance lines are expected at the X band for $\varphi = 90°$, separated by about 40 G, the linewidth prevented the resolution of the observed structure of the spectra into separate lines.

Since the excitation gap is expected to decrease with increasing temperature, ω_G will equal ω_Q at a certain temperature $T_{GQ} > 80$ K. Thus, the lower-field resonance line measured for $\varphi \cong 90°$ in the Q band should shift with T to even lower fields. As shown in Fig. 5, it approaches $H = 0$ for $T_{GQ} \cong 107(5)$ K. Below T_{GQ}, only nonresonant losses at $H \approx 0$ are expected for $\varphi = 0°$. Above this temperature, we observe resonance lines at $H \neq 0$, as seen in Figs. 5 and 6. Notice in Fig. 5 that three resonance lines may be expected for intermediate angles in a narrow temperature interval around T_{GQ}. However, we could not resolve these lines.

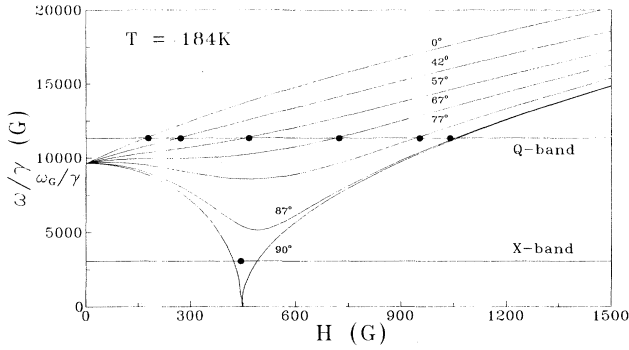The angular variation of the spectra for $T = 184$ K,

FIG. 12. ω/γ vs H curves for the WF resonant mode, calculated for different values of φ using Eq. (5). Horizontal lines indicate the microwave frequencies ω_x/γ and ω_Q/γ and the circles are the experimental data at both frequencies measured for $T=184$ K.

shown in Fig. 9, corresponds to a case where $\omega_G < \omega_Q$. In Fig. 12 we present calculated (ω/γ) vs H curves together with the experimental data taken at this temperature for different values of φ. The parameters used in this case for the fitting are $H_{\mathrm{eff}}^y=4.5(5)\times10^2$ G and $H_{\mathrm{eff}}^z=2.1(2)$ $\times10^5$ G. The solid line shown in Fig. 10 corresponds to the angular dependence calculated with these values. As can be seen, the agreement with the experimental data is also very good at this temperature. The signal at $H=0$ observed between T_{GQ} and $T\approx170$ K for $\varphi\cong90°$ (see Fig. 4) may be interpreted as a nonresonant absorption, as suggested by the field dependence of ω/γ in Fig. 12.

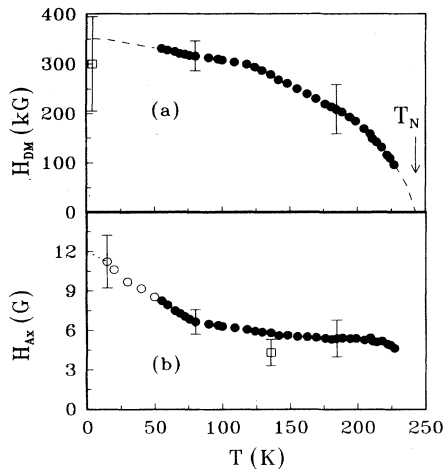From the resonance fields measured at the Q band for

FIG. 13. Anisotropy fields vs T as determined from resonance data (circles): (a) out of plane, $H_{\mathrm{DM}}(T)\cong H_{\mathrm{eff}}^z(T)$, and (b) in plane, $H_{\mathrm{ax}}(T)\cong[H_{\mathrm{DM}}(T)/2H_E(T)]H_{\mathrm{eff}}^y(T)$. The dashed lines are guides to the eye and the open circles correspond to values calculated from $H_{\mathrm{eff}}^y(T)$ and extrapolated values for $H_{\mathrm{DM}}(T)$. The squares correspond to values obtained from dc-magnetization measurements of Ref. 12.

$\varphi=0°$ and $\varphi=90°$ (see Fig. 5) and for $\varphi=90°$ at the X band, we derived the temperature dependence of the effective anisotropy fields. The out-of-plane effective anisotropy field H_{eff}^z decreases continuously with temperature, vanishing around $T_N\cong243$ K, as shown in Fig. 13(a). The in-plane anisotropy field, which is given approximately by the resonance field at the X band, presents a minimum at $H_{\mathrm{eff}}^y\cong400$ G for $T\approx130$ K, as seen in Fig. 2. This value is consistent with that derived from the critical field in dc-magnetization measurements[13] at 135 K, $H_{\mathrm{eff}}^y=H_c\cong340$ G.

D. Line shape and linewidth

An interesting point to discuss is the shape and phase of the observed lines. In a regular EPR experiment made in the absorption mode, the signals are detected through amplitude modulation of the external field and the spectrum is proportional to the field derivative of the absorbed energy. However, in our Q-band experiments angular variations were done by rotating the applied field while keeping the modulation coils fixed to the resonant cavity. This procedure introduces, besides the regular amplitude modulation, an angular modulation of the field[15] in the ab plane. Thus, the amplitude of the signal detected includes two different contributions.

The microwave losses at a fixed frequency $\omega_{\mu w}$ are given as a function of the applied field H by $P(H,\varphi)\propto\omega_{\mu w}\chi''(\omega_{\mu w},H,\varphi)$. Including phenomenological damping into the equations of motion of Sec. III B, as in Ref. 21, results in an approximately Lorentzian line shape, $\chi''(\omega,H,\varphi)=K[(\omega-\omega_r)^2+\Delta\omega_{1/2}^2]^{-1}$, with the resonance frequency $\omega_r(H,\varphi)$ determined by Eq. (5), and a full width at half amplitude $\Delta\omega_{1/2}$, independent of H and φ. If the detection process includes a modulation field δH with components $\delta H_{\|}$ and $\delta H_{\perp}$, parallel and perpendicular to the applied field $\mathbf{H}$, the measured signal is given, for $\delta H_{\|}$, $\delta H_{\perp}\ll H$, by

$$S(H,\varphi)\propto\frac{\partial P(H,\varphi)}{\partial\omega_r}\frac{\partial\omega_r(H,\varphi)}{\partial H}\delta H_{\|}$$
$$+\frac{\partial P(H,\varphi)}{\partial\omega_r}\frac{\partial\omega_r(H,\varphi)}{\partial\varphi}\frac{\delta H_{\perp}}{H}. \tag{8}$$

When the resonant condition $\omega_r(H,\varphi)=\omega_{\mu w}$ is fulfilled for $H=H_r$, we can approximate $\omega_r(H,\varphi)\cong\omega_{\mu w}+(\partial\omega_r/\partial H)|_{H=H_r}(H-H_r)$, if the (ω/γ) vs H curves are reasonably linear in the interval $(\omega_r-\Delta\omega_{1/2},\omega_r+\Delta\omega_{1/2})$. Then, we obtain

$$S(H,\varphi)\cong\frac{(2K\omega_{\mu w})(H_r-H)}{(H-H_r)^2+[\Delta\omega_{1/2}/(\partial\omega_r/\partial H)]^2}$$
$$\times[\delta H_{\|}-(1/H_r)(\partial H_r/\partial\varphi)\delta H_{\perp}]. \tag{9}$$

In this approximation, the line shape is a Lorentzian first derivative also as a function of H, centered in $H=H_r$ and with a peak-to-peak linewidth, $\Delta H_{\mathrm{pp}}=\Delta\omega_{1/2}/|\sqrt{3}\partial\omega_r/\partial H|$. The amplitude of the signal is not only proportional to $\delta H_{\|}$ (amplitude modulation), but has an important contribution due to angular modulation when

the resonance lines are highly anisotropic,[15] i.e., $\partial H_r/\partial\varphi$ is large. The amplitude and phase of the signal is determined in this case by the factor $(1/H_r)\partial H_r/\partial\varphi$.

Then, the different phase of the two Q-band signals measured at $T=80$ K for $\varphi>74°$ (shown in Figs. 4 and 7), can be explained as due to the different sign of their angle derivatives, i.e., the resonance field of one of the signals increases and the other one decreases as φ increases. The angular modulation prefactor is large for $\varphi\approx74°$, but for φ approaching 90°, the angular dependence is strongly reduced and the amplitude of the signals is much smaller. When the same measurements were done keeping the modulation field parallel to H, i.e., only with amplitude modulation, the two signals shown in Fig. 4 had the same phase. However, as the amplitude modulation is less effective for these absorptions than the angular modulation, the signal-to-noise ratio of the detected signal is worse. The direct absorption spectra (measured without any field modulation), in spite of their much lower signal-to-noise ratio that prevented a systematic study of the resonances at all angles, showed that the resonance fields derived from the modulated spectra were coincident with the fields for maximum absorption within experimental uncertainty. For $T=184$ K, the angular variation of the signal amplitude also corresponds closely to $\partial H_r(\varphi)/\partial\varphi$, as shown in the inset of Fig. 10. In conclusion, the angular modulation of a resonance line has a double advantage; it allows one to detect weaker signals and gives information not only on H_r but on its variation with φ; that is, on $\partial H_r(\varphi)/\partial\varphi$. On the other hand, extra care has to be taken when interpreting the amplitude of the observed signals.

From the measured field linewidths at the Q band, and using a numerical estimate for $\partial(\omega/\gamma)/\partial H$, we have determined $\Delta\omega_{1/2}/\gamma\cong1.6(2)$ kG for $T=80$ K. Notice that because $\partial(\omega/\gamma)/\partial H\gg1$ in this case, the measured field linewidths $\Delta H_{pp}=70(5)$ and 55(5) G at $\varphi=90°$ for the low- and high-field lines, are much smaller than $\Delta\omega_{1/2}/\gamma$.

Numerical simulations of the spectra showed that due to this frequency linewidth, the two lines at the X band, separated ≈40 G, are expected to have individual linewidths of about 10 and 17 G, respectively. However, these lines may not be resolved if a misalignment of the sample in a few tenths of a degree would occur (0.5° for χ'' and 0.8° for χ'). In addition, inhomogeneities in the orientation of the [110] axis throughout the crystal would increase the width of the lines, making their resolution more difficult. In our case, only $\chi'(H)$ shows incipient resolution into two lines, as seen in Fig. 3.

The frequency linewidth also determines the angular range where the nonresonant losses around H_{min} should be observed with significant amplitude. The calculated ω/γ vs H curves in Fig. 11 indicate that $(\omega_{min}-\omega_Q)\approx0.65\Delta\omega_{1/2}$ for $\varphi\approx67°$, the lower limit for the existence of the minimum at $T=80$ K, and $(\omega_{min}-\omega_X)\approx\Delta\omega_{1/2}$ for $\varphi\approx88.8°$. These estimations are in qualitative agreement with the experiments, since the nonresonant signal is observed in the Q band for the whole interval $67°\le\varphi\le74°$, while it is only observed in a very narrow region[12] around

$\varphi=90°$ in the X band. For these nonresonant losses, the linearization condition used when deriving Eq. (9) is not satisfied and the line shape of the signals need not be Lorentzian. Numerical simulations indicate that $\partial P/\partial\omega$ remains approximately constant in Eq. (8) for $H\approx H_{min}$ and the main contribution to $S(H,\varphi)$ is proportional to $(\partial\omega_{min}/\partial\varphi)$, which presents a single maximum for $H\cong H_{min}$. We can then understand the line shape of the signals measured for $67°\le\varphi\le74°$ shown in FIg. 7, and justify the assumption that H_{min} is given by the field for maximum signal amplitude.

The observed temperature variations of $\Delta H_{pp}(T)$ for 15 K $<T<$ 200 K, both in the X and Q bands, are mainly related to changes of $\partial(\omega/\gamma)/\partial H$ due to the temperature variation of H_{eff}^z and H_{eff}^y, rather than to a temperature dependence of $\Delta\omega_{1/2}$. Thus, the derived value for $\Delta\omega_{1/2}$ is almost temperature independent and may also be used to estimate the temperature interval where the $H\cong0$ nonresonant lines should be observed. In the case of $\varphi=0°$, the nonresonant signal is present when $\omega_G>\omega_Q$ and significant intensity is expected for $T<T_{GQ}$, until $\omega_G(T)-\omega_Q\approx\Delta\omega_{1/2}$, which occurs at $T\cong60$ K. At this temperature the measured signal has been reduced to less than 10% of its intensity around T_{GQ}. For $\varphi=90°$, a nonresonant absorption may be observed for $T>T_{GQ}$ until $\omega_Q-\omega_G(T)\approx\Delta\omega_{1/2}$. This occurs at $T=165$ K and the measured intensity is, in this case, about 15% of its maximum amplitude near T_{GQ}. Notice that Eq. (8) predicts, for these nonresonant losses around $H=0$, that $S(H)$ should be an odd function of H, in agreement with the experiments.

V. CONCLUSIONS

We have presented a detailed experimental study of the magnetic-resonance absorptions in single-crystal samples of Eu$_2$CuO$_4$, slightly doped with Gd. We have used a phenomenological model for the magnetic free energy which describes the compound as an anisotropic WF with two effective parameters, $H_{eff}^y(T)$ and $H_{eff}^z(T)$. Excellent agreement between the calculated and measured magnetic-resonance fields is obtained. The resulting anisotropy fields are consistent with dc-magnetization data.[13] Within this picture, the anomalous microwave absorption signal observed[12] at the X band can be explained as due to a softening of the WF mode in the spin reorientation transition induced by the applied field. The frequency of this WF mode is zero when H is applied perpendicular to the easy axis and equal to $H_C=H_{eff}^y$. This is the critical field necessary for the alignment of the WF component with H. A more complex and richer behavior is found at the Q band, including the observation of two separate absorptions or a single one, depending on whether the magnetic excitation anisotropy gap is smaller or larger than the microwave frequency. The angular dependence of the experimental data is also correctly described by the phenomenological model. The temperature dependence of the effective magnetic anisotropy fields has been determined.

The effective fields $H_{eff}^y(T)$ and $H_{eff}^z(T)$ have been relat-

ed to the anisotropy fields of the AF two-sublattice model, $H_{DM}(T)$ and $H_{ax}(T)$, using Eq. (4) with $H_E(T) = H_E(0)M_0(T)/M_0(0)$, taking $M_0(T)$ from Ref. 23 and neglecting the contributions from H_{az}. The extrapolated values for $T=0$ are $H_{DM}(0)=3.5(5)\times10^5$ G and $H_{ax}(0)=12(2)$ G. The values obtained for $H_{DM}(T)$ and $H_{ax}(T)$ are given in Fig. 13. For $T=135$ K, they agree with those derived from dc-magnetization measurements.[13]

The line shape of the signals has been analyzed in terms of a temperature-independent frequency linewidth $\Delta\omega_{1/2}$. The effects on the line shape and phase of both amplitude and angular modulation of the external field have been discussed.

The phenomenological model used includes the fact that a WF component is induced after field cooling the samples, with a uniaxial magnetic anisotropy along $[110]_{FC}$. However, a microscopic description of the effect of field cooling is still missing. Coffey discussed[26] the role of crystalline distortions in the WF behavior of La_2CuO_4, showing the need of a particular order of the lattice distortions for the existence of macroscopic weak ferromagnetism. The EPR spectra of the dilute Gd^{3+} ions[6] indicate the displacement of the oxygen ions from their tetragonal positions and our present results suggest that some degree of order in these lattice distortions is induced by field cooling the samples, favoring an anisotropy axis along the $\langle110\rangle$ direction lying close to $\mathbf{H}_{FC}$. The differences found[6] between the Gd^{3+} EPR spectra of ZFC and FC samples support the mechanism proposed. In compounds where the WF is well established and crystal superstructures have been observed,[8] such as Gd_2CuO_4, the differences between field cooling and zero-field cooling on their properties are much smaller.[14]

*Present address: Max Planck Institut für Festkörperforschung, Heisenbergstrasse 1, D-7000 Stuttgart 80, Germany.

†Present address: Istituto di Teoria e Struttura Elettronica, Area della Ricerca di Roma, CP 10, I-00016 Monterotondo Stazione, Roma, Italy.

‡Commisión Nacional de Energía Atómica and Universidad Nacional de Cuyo.

[1] R. Saez-Puche, M. Norton, and W. S. Glausinger, Mater. Res. Bull. **17**, 1523 (1982); R. Saez-Puche, M. Norton, T. R. White, and W. S. Glausinger, J. Solid State Chem. **50**, 281 (1983); R. Saez-Puche, J. C. Grenier, and W. S. Glausinger, An. Quim. **80**, 28 (1984).

[2] S. B. Oseroff, D. Rao, F. Wright, M. Tovar, D. C. Vier, S. Schultz, J. D. Thompson, Z. Fisk, and S.-W. Cheong, Phys. Rev. B **41**, 1934 (1990).

[3] L. B. Steren, M. Tovar, and S. B. Oseroff, Phys. Rev. B **46**, 2874 (1992).

[4] M. B. Maple, N. Y. Ayoub, J. Beille, T. Bjørnholm, Y. Dalichaouch, E. A. Early, S. Ghamaty, B. W. Lee, J. T. Markert, J. J. Neumeier, G. Nieva, L. M. Paulius, I. K. Schuller, C. L. Seaman, and P. K. Tsai, Prog. High Temperature Supercond. **25**, 536 (1990); P. Adelmann, R. Ahrens, G. Czjzek, G. Roth, H. Schmidt, and C. Steinleitner, Phys. Rev B **46**, 3619 (1992).

[5] Hk. Müller-Buschbaum and W. Wollschläger, Z. Anorg. Allg. Chem. **414**, 76 (1975).

[6] R. D. Zysler, M. Tovar, C. Rettori, D. Rao, H. Short, S. B. Oseroff, D. C. Vier, S. Schultz, Z. Fisk, and S.-W. Cheong, Phys. Rev. B **44**, 9467 (1991).

[7] Ph. Galez, P. Schweiss, G. Collin, and R. Bellissent, J. Less-Common Met. **164&165**, 784 (1990).

[8] P. Bordet, J. J. Capponi, C. Chaillout, D. Chateigner, J. Chenavas, Th. Fournier, J. L. Hodeau, M. Marezio, M. Perroux, G. Thomas, and A. Varela-Losada, Physica C **193**, 178 (1992).

[9] M. L. Laguna, M. L. Sanjuán, M. Tovar, and Z. Fisk (unpublished).

[10] I. Dzyaloshinsky, J. Phys. Chem. Solids **4**, 241 (1958); T. Moriya, in *Magnetism,* edited by G. T. Rado and H. Suhl (Academic, New York, 1966), Vol. 1, p. 85.

[11] M. Tovar, X. Obradors, F. Pérez, S. B. Oseroff, R. J. Duro, J. Rivas, D. Chateigner, P. Bordet, and J. Chenavas, Phys. Rev. B **45**, 4729 (1992).

[12] D. C. Vier, S. Schultz, C. Rettori, D. Rao, S. B. Oseroff, M. Tovar, Z. Fisk, and S.-W. Cheong, J. Appl. Phys. **69**, 4873 (1991).

[13] R. D. Zysler, A. Butera, A. Fainstein, and M. Tovar, J. Appl. Phys. **73**, 5680 (1993).

[14] J. D. Thompson, S.-W. Cheong, S. E. Brown, Z. Fisk, S. B. Oseroff, M. Tovar, D. C. Vier, and S. Schultz, Phys. Rev. B **39**, 6660 (1989). Samples grown in Pt crucibles show a small (less than 1%) Pt contamination.

[15] E. Edgar, J. Phys. E **8**, 179 (1975).

[16] Eu_2CuO_4 doped with 0.5 at. % Y presents similar properties, i.e., the Gd magnetic moment is not an important factor for the data reported here.

[17] F. B. Hagedorn, E. M. Gyorgy, R. C. LeCraw, J. C. Hensel, and J. P. Remeika, Phys. Rev. Lett. **21**, 364 (1968).

[18] P. Pincus, Phys. Rev. Lett. **5**, 13 (1960).

[19] G. H. Herrmann, J. Phys. Chem. Solids **24**, 597 (1963).

[20] J. R. Shane, Phys. Rev. Lett. **20**, 728 (1968).

[21] F. B. Hagedorn and E. M. Gyorgy, Phys. Rev. **174**, 540 (1968).

[22] Tineke Thio, C. Y. Chen, B. S. Freer, D. R. Gabbe, H. G. Jenssen, M. A. Kastner, D. J. Piccone, N. W. Preyer, and R. J. Birgeneau, Phys. Rev. B **41**, 231 (1990).

[23] M. Matsuda, K. Yamada, K. Kakurai, H. Kadowaki, T. R. Thurston, Y. Endoh, Y. Hidaka, R. J. Birgeneau, M. A. Kastner, P. M. Gehring, A. H. Moudden, and G. Shirane, Phys. Rev. B **42**, 10 098 (1990).

[24] Y. Ohta, T. Toyama, and S. Maekana, Phys. Rev. Lett. **66**, 1228 (1991), and references therein.

[25] When the signals are distorted or superimposed we have chosen the individual resonance fields at half amplitude of the derivative signals. Since the lines are relatively narrow, the systematic errors introduced are expected to be small.

[26] D. Coffey, T. M. Rice, and F. C. Zhang, Phys. Rev. B **44**, 10 112 (1991).